

# Paramagnetic Meissner effect in superconductors from self-consistent solution of Ginzburg–Landau equations

G.F. Zharkov

*P.N. Lebedev Physics Institute, Russian Academy of Sciences, Moscow, 117924, Russia*  
(July, 2000)

The paramagnetic Meissner effect (PME) is observed in small superconducting samples, and a number of controversial explanations of this effect are proposed, but there is as yet no clear understanding of its nature. In the present paper PME is considered on the base of the Ginzburg-Landau theory (GL). The one-dimensional solutions are obtained in a model case of a long superconducting cylinder for different cylinder radii  $R$ , the GL-parameters  $\kappa$  and vorticities  $m$ . According to GL-theory, PME is caused by the presence of vortices inside the sample. The superconducting current flows around the vortex to screen the vortex internal field from the bulk of the sample. Another current flows at the boundary to screen the external field  $H$  from entering the sample. These screening currents flow in opposite directions and contribute with opposite signs to the total magnetic moment (or magnetization) of the sample. Depending on  $H$ , the total magnetization  $M$  may be either negative (diamagnetism), or positive (paramagnetism). The detailed study of a very complicated saw-like dependence  $M(H)$  (and of other characteristics), which follow from the self-consistent solutions of the GL-equations, is presented.

## I. INTRODUCTION

A superconductor, placed in magnetic field and cooled down through the transition temperature, expels the magnetic flux. This phenomenon, known as the diamagnetic Meissner effect (DME), is one of the most essential properties of superconductors. Surprisingly, several recent experiments have shown that some superconducting samples may attract magnetic field, which corresponds to the so-called paramagnetic Meissner effect (PME). Originally, PME was observed in small size high-temperature superconductors (HTS), what has prompted the appearance of a number of theories, attributing this effect to a non-conventional superconductivity in these materials. (Mention such explanations, as spontaneous currents due to  $\pi$ -contacts, vortex pair fluctuations,  $d$ -wave superconductivity, orbital glass, the Josephson junctions, the Andreev reflection of pairs at the boundary, and others. The numerous references to the experimental and theoretical work on PME may be found in recent papers [1–7].) Later, the anomalous PME was observed also in conventional low- $T_c$  superconductors and was considered as intrinsic property of any finite-size superconductor.

In [2–5] the PME was studied in a case of conventional superconductors, using the Ginzburg–Landau (GL) system of equations. Here such conceptions were put forward, as the flux capture and its compression [2], the hysteresis transitions and the role of experimental setup [3], the metastability of the vortex configuration due to the influence of the sample surface [4], the disbalance of screening currents in metastable vortex states [5].

As was noticed in [5], the GL-theory treats PME in finite-size superconductors as purely electrodynamic ef-

fect, caused by presence of vortices inside the superconductor. If the vortex exists inside the sample, the superconducting current  $j_s$  flows around the vortex center in a direction to screen out the vortex field from entering the bulk of the sample. If the sample is placed in external magnetic field  $H$ , the additional surface current flows to screen out the field  $H$  from entering the sample. These two currents have opposite directions and produce contributions of opposite sign to the sample magnetic moment (or, magnetization)  $\mathbf{M} = (1/2c) \int [\mathbf{j}_s \times \mathbf{r}] dv$ . The resulting value of  $M$  (in the direction of  $H_z > 0$ ) may be either negative (this corresponds to diamagnetic susceptibility), or positive (this corresponds to paramagnetic susceptibility), depending on  $H$  magnitude.

In the present paper the origination of PME within the GL-theory approach is studied in more details, as compared with [5], including both type-I and type-II superconductors, for various sample dimensions and different values of GL-parameter  $\kappa$ . In Sec. 2 the GL-equations for the order parameter  $\psi$  and magnetic field  $B$  inside the superconductor are written. In Sec. 3 the results of numerical calculations of non-linear system of equations are presented by a number of graphics, accompanied by necessary comments. Sec. 4 contains a short resume and discussion of the results.

## II. EQUATIONS

Below the case is considered of a long superconducting cylinder of radius  $R$ , in the external magnetic field  $H \geq 0$ , which is parallel to the cylinder element. In the cylindrical co-ordinates the system of GL-equations may

be written in dimensionless form [5]

$$\frac{d^2U}{d\rho^2} - \frac{1}{\rho} \frac{dU}{d\rho} - \psi^2 U = 0, \quad (1)$$

$$\frac{d^2\psi}{d\rho^2} + \frac{1}{\rho} \frac{d\psi}{d\rho} + \varkappa^2(\psi - \psi^3) - \frac{U^2}{\rho^2}\psi = 0. \quad (2)$$

Here  $U(\rho)$  is the dimensionless field potential;  $b(\rho)$  is the dimensionless magnetic field;  $\psi(\rho)$  is the normalized order parameter;  $\rho = r/\lambda$ ,  $\lambda$  is the field penetration length;  $\lambda = \varkappa\xi$ , where  $\xi$  is the coherence length,  $\varkappa$  is the GL-parameter. The dimensioned potential  $A$ , field  $B$  and current  $j_s$  are related to the corresponding dimensionless quantities by the formulae [5]:

$$A = \frac{\phi_0}{2\pi\lambda} \frac{U+m}{\rho}, \quad B = \frac{\phi_0}{2\pi\lambda^2} b, \quad b = \frac{1}{\rho} \frac{dU}{d\rho},$$

$$j(\rho) = j_s / \frac{c\phi_0}{8\pi^2\lambda^3} = -\psi^2 \frac{U}{\rho}, \quad \rho = \frac{r}{\lambda}. \quad (3)$$

(The field  $B$  in (3) is normalized by  $H_\lambda = \phi_0/(2\pi\lambda^2)$ , with  $b = B/H_\lambda$ ; instead of  $H_\lambda$  one can normalize by  $H_\xi = \phi_0/(2\pi\xi^2)$ , or by  $H_\varkappa = \phi_0/(2\pi\xi\lambda) = H_\xi/\varkappa$ . The coefficients in (1), (2) would change accordingly.) The vorticity  $m$  in (3) specifies how many flux quanta are associated with the vortex, centered at the cylinder axis (the giant-vortex state).

The boundary conditions to Eq. (1) are [5]:

$$U|_{\rho=0} = -m, \quad \left. \frac{dU}{d\rho} \right|_{\rho=\rho_1} = h_\lambda. \quad (4)$$

where  $\rho_1 = R/\lambda$ ,  $h_\lambda = H/H_\lambda$ .

The boundary conditions to Eq. (2) are [5]:

$$\left. \frac{d\psi}{d\rho} \right|_{\rho=0} = 0, \quad \left. \frac{d\psi}{d\rho} \right|_{\rho=\rho_1} = 0 \quad (m=0),$$

$$\psi|_{\rho=0} = 0, \quad \left. \frac{d\psi}{d\rho} \right|_{\rho=\rho_1} = 0 \quad (m>0). \quad (5)$$

The magnetic moment (or, magnetization) of the cylinder, related to the unity volume, may be written in a form

$$\frac{M}{V} = \frac{1}{V} \int \frac{B-H}{4\pi} dv = \frac{B_{av} - H}{4\pi},$$

$$B_{av} = \frac{1}{V} \int B(\mathbf{r}) dv = \frac{1}{S} \Phi_1,$$

where  $B_{av}$  is the mean field value inside the superconductor,  $\Phi_1$  is the total magnetic flux, confined in the cylinder. In the normalization (3), denoting  $\bar{b} = B_{av}/H_\lambda$ ,  $h_\lambda = H/H_\lambda$ ,  $M_\lambda = M/H_\lambda$ , one finds

$$4\pi M_\lambda = \bar{b} - h_\lambda, \quad \bar{b} = \frac{2}{\rho_1^2} (U_1 + m), \quad (6)$$

$$\phi_1 = \frac{\Phi_1}{\phi_0} = U_1 + m, \quad U_1 = U(\rho_1), \quad \rho_1 = \frac{R}{\lambda}.$$

Accordingly, the normalized Gibbs free energy of the system may be written as [5]

$$\Delta g = \Delta G / \left( \frac{H_{cm}^2}{8\pi} V \right) = g_0 - \frac{8\pi M_\lambda}{\varkappa^2} h_\lambda + \frac{4m}{\varkappa^2} \frac{b(0) - h_\lambda}{\rho_1^2},$$

$$g_0 = \frac{2}{\rho_1^2} \int_0^{\rho_1} \rho d\rho \left[ \psi^4 - 2\psi^2 + \frac{1}{\varkappa^2} \left( \frac{d\psi}{d\rho} \right)^2 \right]. \quad (7)$$

Here  $\Delta G = G_s - G_n$  is the difference of free energies in superconducting and normal states;  $b(0) = B(0)/H_\lambda$ ,  $B(0)$  is the magnetic field at the cylinder axis;  $H_{cm} = \phi_0/(2\pi\sqrt{2}\lambda\xi)$  is thermodynamical critical field of massive superconductor;  $g_0$  is the condensation energy with account for the order parameter gradient. The expressions (6), (7) will be used below for calculating the corresponding quantities.

### III. NUMERICAL RESULTS

The system of equations (1), (2) was solved numerically by the method, described in [5,8]. For every fixed set of parameters  $R, H, m, \varkappa$  the unique self-consistent solution for  $\psi(\rho)$  and  $U(\rho)$ , satisfying the boundary conditions (4), (5), was found. If the external field  $H$  exceeds some critical value  $H_c^{(m)}$  ( $H > H_c^{(m)}$ ), no superconducting solution with  $\psi \neq 0$  is possible. The phase diagrams, which separate the superconducting ( $\psi \neq 0$ ) and normal ( $\psi \equiv 0$ ) regions, are presented in Fig. 1 for different vorticities  $m$  and parameters  $\varkappa$ .

The critical field of the vortex-free Meissner state ( $m = 0$ ) is distinguished by thick curve. The superconducting region lays between this curve and the axis  $h_\xi = 0$  ( $h_\xi = H/H_\xi$ ). For  $m > 0$  the superconducting region is inside of the corresponding  $m$ -curve (thin line). To every point of the superconducting  $m$ -region corresponds some solution of Eqs. (1)–(5). The transformation of solutions, when the superconducting regions are crossed along the lines  $R_\lambda \equiv R/\lambda = \text{const}$  (see the dotted horizontal lines), is illustrated below by Figs. (2)–(4).

In Figs. 1(a, b) the dotted vertical line  $h_\xi = 1.695$  represents the critical field  $H_{c3} = 1.695H_{c2}$  ( $H_{c2} = \phi/(2\pi\xi^2) \equiv H_\xi$ ), at which the surface superconductivity [9,10] nucleates in large ( $R_\lambda \gg 1$ ) samples. It is seen, that in type-II superconductors ( $\varkappa > 1/\sqrt{2}$ ) the superconducting states ( $m > 0$ ) are possible, which lay to the right of the line  $m = 0$ . One may say, that these states are enhanced by the external field. In contrast to this, in type-I superconductors (see Fig. 1(c)) the states  $m > 0$

lay to the left of the line  $m = 0$ , so they are weakened by the field.

Fig. 2 illustrates the superconductor behavior ( $R_\lambda = 2$ ,  $\varkappa = 2$ ), when the field  $h_\xi$  varies. In Fig. 2(a) the regions are depicted, where the state  $m$  can exist ( $\psi_{max}$  is the maximal value of the order parameter in the corresponding  $m$ -state). For instance, the state  $m = 4$  (which is distinguished for clarity by thick line) can exist only in the interval of fields, where  $\psi_{max} > 0$ . The state  $m = 11$  can exist only in sufficiently large fields,  $h_\xi \sim 2$  (see also Fig. 1(a)).

Fig. 2(b) shows the field dependence of the cylinder magnetization in different  $m$ -states. For instance, the magnetization ( $-4\pi M_\lambda$ ) in the state  $m = 4$  may be either positive (this corresponds to diamagnetic susceptibility,  $M_\lambda < 0$ ), or negative (this corresponds to paramagnetic susceptibility,  $M_\lambda > 0$ ), depending on the field value. The vortex-free Meissner state ( $m = 0$ ) is diamagnetic for all fields.

Fig. 2(c) shows the normalized free-energy difference,  $\Delta g$ , for the states with different  $m$ . At the points, where the curves with neighboring values of  $m$  cross each other (marked by open circles), the equilibrium transitions between the states  $m$  and  $m \pm 1$  became possible. These equilibrium transitions are marked by the dashed vertical lines in Fig. 2(b). If the equilibrium transitions are only allowed, the magnetization curve would always be diamagnetic ( $-4\pi M_\lambda > 0$ ), and have a reversible saw-like shape. However, if the metastable states are also allowed, the magnetization curve would look very different. This is illustrated by Figs. 3(a,b,c) for  $\varkappa = 1$  and by Figs. 3(d,e,f) for  $\varkappa = 0.5$ .

Consider Fig. 3(c), the state  $m = 2$ . That part of the curve  $m = 2$ , which lays to the left of the equilibrium point ( $eq$ ), is metastable (because the lower energy states  $m = 0$ , or  $m = 1$ , exist). If the field  $h_\xi$  is diminished from its equilibrium value (in the field-cooling regime), the state  $m = 2$  can persist only down to the point  $\alpha$ , where the forced transition to other state should occur. The nearest laying energy state is  $m = 1$ , it corresponds to the relative minimum of the free energy (the state  $m = 0$  corresponds to the absolute minimum). If the transitions between the nearest laying energy minima are possible, then at the point  $\alpha$  the transition from the state  $m = 2$  to the state  $m = 1$  may occur. In Fig. 3(b) this would mean the transition from the paramagnetic state  $m = 2$  (which lays to the left of the dashed-dotted vertical line, passing through the point  $-4\pi M_\lambda = 0$ ) to the paramagnetic state  $m = 1$ . If the field  $h_\xi$  is now increased, the state  $m = 1$  may survive up to the point  $\delta$ , where the forced transition from the diamagnetic state  $m = 1$  to the diamagnetic state  $m = 3$  may occur. At the point  $\beta$  the transition from paramagnetic part of the curve  $m = 3$  to the paramagnetic part of the curve  $m = 2$  occurs. At the point  $\gamma$  the transition between diamagnetic ( $m = 0$ ) and paramagnetic ( $m = 3$ ) states may happen. Note,

that all paramagnetic states are metastable (they lay to the left of the corresponding equilibrium points). Evidently, the transitions between various states, shown in Figs. 3(a,b,c), may lead to the hysteresis behavior of  $M(H)$  (see also [3,4]).

[Note, that for larger values of  $R_\lambda$  and  $\varkappa$  the reversible jump transitions to the edge-suppressed states [5] of the same vorticity  $m$  are also possible, which might additionally complicate the dependence  $M(H)$ .]

The analogous transitions between paramagnetic and diamagnetic states are also possible in type-I superconductors (see Figs. 3(d,e,f)). Notice, that the curve  $m = 0$  terminates at the point  $\gamma$ , where  $\Delta g > 0$ . This part of the curve corresponds to the "superheated" superconducting state, considered first by Ginzburg [11] for type-I superconductors in the approximation  $\psi = \text{const}$  (see also [12]). The point  $\gamma$  corresponds to the maximal superheating. The only possible transition here may be to the normal state ( $\psi = 0$ ). If the field  $h_\xi$  is now diminished, the normal state may be "supercooled" [11,12] down to the point  $\delta$  ( $h_\xi = 1.49$ ), where the superconducting state recovers. The arrows in Fig. 3(d) mark the boundary of the hysteresis loop. (The supercooled states exist also in a case  $\varkappa > 1/\sqrt{2}$ . They additionally complicate the picture and are not shown in Figs. 3(a,b,c).)

As is seen from Figs. 2,3, each magnetization curve ( $-4\pi M_\lambda^{(m)}$ ) has the diamagnetic and paramagnetic parts. Consider points of maximal diamagnetism and maximal paramagnetism. Fig. 4 illustrates the space distributions  $\psi(r)$ ,  $b(r)$ ,  $j(r)$  at these points for several values of  $m, \varkappa, R_\lambda$ . The curves 1 (thick lines in Fig. 4) correspond to maximal paramagnetism ( $M_\lambda > 0$ ), the curves 3 (thin lines) correspond to maximal diamagnetism ( $M_\lambda < 0$ ), the curves 2 (dashed lines) represent points, where  $M_\lambda = 0$ .

Figs. 4(b,e,h) show, that for paramagnetic curves 1 the magnetic field inside the sample is greater, than the applied field  $h_\lambda$  ( $b(r) > h_\lambda$ ,  $h_\lambda = \varkappa^2 h_\xi$ ). This means, that the influence of the internal vortex field  $B(0)$  is greater, than the influence of the external field  $H$ . The relative suppression of the order parameter, seen for the curves 1 in Figs. 4(a,d,g), is caused mainly by the internal field  $B(0)$ . The same is seen in Figs. 4(c,f,i), where all the currents 1 are paramagnetic ( $j > 0$ ), they screen mainly the internal vortex field.

For larger fields  $H$  (the curves 2), the role of external magnetic field is more pronounced. Now, partly  $b(r) > h_\lambda$  (the paramagnetic behavior), and partly  $b(r) < h_\lambda$  (the diamagnetic behavior). Analogously behaves the current  $j$ : part of the current is  $j > 0$  (paramagnetic screening of the vortex field), and partly  $j < 0$  (diamagnetic screening of the external field). These two parts of  $j$  counterbalance each other, resulting in zero magnetization,  $M_\lambda = 0$ .

The order parameter  $\psi(r)$  in the case 2 is enhanced by

a larger field (compare the curves 2 and 1 for  $\psi$ ). This reflects the reentrant behavior of small-size samples: the superconductivity, which was impossible in small external field, is possible again in larger fields (see Figs. 2,3).

When the field  $H$  is increased further (the curves 3 in Fig. 4), the sample passes to diamagnetic state ( $M_\lambda < 0$ ): the field  $b(r) < h_\lambda$  everywhere, the current  $j$  screens predominantly the external field ( $j(r) < 0$  near the surface), the order parameter  $\psi(r)$  displays the suppression by strong external field  $H$ .

In the foregoing discussion the case was considered, when the external field  $H$  has been varied, but the temperature  $T$  was fixed (see the horizontal dotted lines  $T = \text{const}$  in Fig. 1). In some experiments (for instance, [7]) the field  $H$  was fixed, but the temperature  $T$  varied. In this case the transitions between different diamagnetic and paramagnetic states (see Figs. 3(b,c)) are also possible.

Indeed, in the vicinity of  $T_c$  the parameters  $\xi$  and  $\lambda = \varkappa\xi$  depend on the sample temperature  $T$  by the law  $\xi(T) = \xi_0(1 - T/T_c)^{-1/2}$ . Using notations:  $t = T/T_c$ ,  $R_\lambda = R/\lambda$ ,  $h_\xi = H/H_{\xi_0}$ ,  $H_{\xi_0} = \phi_0/(2\pi\xi_0^2)$ , one has two relations:  $R_\lambda = r_0\sqrt{1-t}$  and  $h_\xi = h_0/(1-t)$ , or

$$1 - t = \frac{R_\lambda^2}{r_0^2} = \frac{h_0}{h_\xi}, \quad (8)$$

where  $r_0 = R/\lambda_0$ ,  $h_0 = H/H_{\xi_0}$ ,  $H_{\xi_0} = \phi_0/(2\pi\xi_0^2)$ ,  $\lambda_0 = \varkappa\xi_0$ . From Eqs. (8) the dependence between  $R_\lambda$  and  $h_\xi$  follows:

$$R_\lambda = \frac{A}{\sqrt{h_\xi}}, \quad A = \frac{R}{\lambda_0} \left( \frac{H}{H_{\xi_0}} \right)^{1/2} \equiv \frac{1}{\varkappa} \left( \frac{2\pi R^2 H}{\phi_0} \right)^{1/2}. \quad (9)$$

The dashed curves in Fig. 1(b) are the lines, along which the representation point  $(R_\lambda, h_\xi)$  moves, when  $H = \text{const}$  and the temperature  $T$  varies only. Taking  $\varkappa = 1$ ,  $H = 100$  Oe, one has  $A = 1$  for  $R = 1.8 \cdot 10^{-5}$  cm, and  $A = 3$  for  $R = 5.4 \cdot 10^{-5}$  cm. Notice the essential difference in the dashed curves positions. For smaller  $R$  ( $A = 1$ ) the system remains mainly in the diamagnetic state  $m = 0$ , so no PME is possible. For larger  $R$  ( $A = 3$ ) the dashed curve  $H = \text{const}$  crosses several of  $m$ -state phase boundaries. This more complicated situation is illustrated by Fig. 5.

In Fig. 5 the temperature dependencies are shown: of the order parameter  $\psi_{max}^{(m)}$ , of the magnetization  $(-4\pi M_\lambda^{(m)})$ , and the Gibbs free energy  $\Delta g^{(m)}$  in several  $m$ -states. It is seen, that the first superconducting state ( $\psi \neq 0$ ), encountered in the temperature-cooled mode, is  $m = 2$  (see Fig. 1(b), the point  $\mu$ ). This is the state of the surface superconductivity in a finite-dimension sample. The magnetization curve is diamagnetic ( $M_\lambda^{(2)} < 0$ ), it starts from zero, as the second order phase transition. When the temperature  $t = T/T_c$  is reduced further, other  $m$ -states became possible. If the temperature  $t$  is swept

up and down (as in [7]), alongside with the equilibrium transitions between diamagnetic states (at the points  $\alpha$  and  $\beta$  in Figs. 5(b,c)) the transitions between various metastable branches of the curves may also occur. For instance, at the termination point  $\gamma$  the jump transition from the diamagnetic state  $m = 0$  to the nearest energy laying paramagnetic state  $m = 4$  is possible; at the termination point  $\delta$  the jump from the paramagnetic state  $m = 4$  to the diamagnetic state  $m = 1$  may occur. The up and down arrows at the points  $\gamma$  and  $\delta$  in Fig. 5(b) mark the possible hysteresis loop in the  $M(T)$ -dependence (compare with the experimentally found dependencies [7]).

A more detailed comparison of the present calculations with experiments on PME is not possible, because the model case of a long circular cylinder approximates the real specimens geometry very crudely. However, it is instructive to see the results of GL-theory, because they suggest some ideas, which should be viewed with attention. For instance, in the scope of GL-theory the PME looks more like a bulk effect, it is caused by the balance of currents, flowing inside the sample. The role of the surface seems not to be crucial, though in the finite-height extended samples [7] the role of the boundary may be important. It also looks probable, that PME might be observed in the proximity structures [6], where the superconducting cylinders are embodied into the normal-metal environment, or in a system of microholes inside the superconducting matrix [13].

Below are comments on some of the papers, where the PME was first considered within the GL-approach.

In [15] the hypothesis was put forward of a normal layer, which might be formed inside the superconducting plate under the influence of the external field  $H$  and is situated at some distance from the plate boundary. According to [15], the conception of such a layer might help in understanding the nature of PME in superconductors. Note, that in the homogeneous GL-theory no such layer is possible, though the basic idea of [15] is, probably, correct. Indeed, if a chain of vortices is formed near the plate surface (with the order parameter vanishing at their axes), the average vortices distribution may be visualized as a normal layer, in accordance with [15].

In [2] the conception of the flux compression was proposed to explain the PME. According to [2], the giant  $m$ -vortex state, which is formed at sufficiently high field  $H$ , persist at smaller  $H$  in a form of the flux-compressed state, with the eventual onset of the paramagnetic response. Some evidence of the possible PME in a small-radius cylinder was obtained in [2] by self-consistent solution of GL-equations. Note, that our calculations are along the same lines (see Figs. 2, 3 and also [5]), but they show, that the giant  $m$ -vortex state can persist only in a finite field interval, outside which the vorticity  $m$  changes. As it follows from Figs. 4(b,e,h), the imposition of the external field  $H$  leads not to a field com-

pression, but, better to say, to a field submission effect. Indeed, at smaller  $H$  (the curves 1) the external field is effectively screened out ( $b(r) > h_\lambda$ ); at larger  $H$  (the curves 2) the Meissner screening is not so effective and the external field is partly submitted into the sample ( $h_\lambda > b(r)$  near the boundary); still at larger  $H$  (the curves 3) the external field floods almost all the interior ( $h_\lambda > b(r)$  everywhere), with eventually total submission to the external field ( $b(r) = h_\lambda$  in the normal state). As was mentioned above, the appearance of PME in this picture is due to the redistribution of the screening currents, flowing inside the specimen.

[There exist some doubts concerning the self-consistency of the solutions, found numerically in [2]. Thus, in Fig. 4(a) [2] the order parameter must depend linearly on  $r$  for  $r \ll 1$ . The local induction  $b(r)$  in Figs. 4(c) and 5(a) [2] is maximal not at  $r = 0$  (where the vortex axis is situated), but at some distance  $r \neq 0$ , which seems strange, etc. Most closely our calculations correlate with those in [3,4,15], where many fragments of the picture, presented above, may be found, though no concise formulation of a possible nature of PME in conventional superconductors was given.]

#### IV. CONCLUSIONS AND DISCUSSION

The GL-theory of a long superconducting cylinder, which accounts for the transitions between centrally symmetric  $m$ -states (the giant-vortex states), gives only qualitative picture of the processes inside the real superconductor. In reality, the giant-vortex may split itself into the asymmetric multi-vortex configuration of the same vorticity  $m$ . The specimen finite height in  $z$ -direction, and the boundary conditions at the surface, might also be important for calculating the real vortex structure. All this makes the analysis more difficult. [The approximate GL-description of the multi-vortex configurations in mesoscopic 3-dimensional samples may be found in [3,4].] However, even in a general case of arbitrary vortex configuration, there will be two currents, flowing in opposite directions: one - to screen out the combined fields of the vortices, and second - to screen out the external field. Thus, basing on the GL-model calculations, it seems reasonable to offer the following qualitative scenario for the appearance of PME in finite-dimension samples.

According to GL-theory, the paramagnetism in conventional low- $T_c$  superconductors may be caused by the presence of vortices inside the superconductor. The vortices, which are formed inside the sample in the field-cooling regime, may be pinned to the boundary, which is a source of inhomogeneity. The directions of the external and of the vortex magnetic fields are the same, but the directions of currents, which flow to screen these fields from the bulk of the sample, are opposite (clockwise and counter clock-wise). The screening currents are

responsible for two contributions of opposite sign to the total magnetic moment (or, equivalently, magnetization) of the sample:  $M = M_{para} + M_{dia}$ . The distributions of the fields and currents inside the sample varies with  $H$ , so the measured magnetization may be either positive ( $M > 0$ , PME), or negative ( $M < 0$ , DME), or  $M = 0$ , depending on  $H$ .

The pinning of the vortices to the boundary is a non-linear effect, described by the system of GL-equations. Each of the vortex configurations of fixed vorticity  $m$  can exist only within a limited interval of fields  $H$ . When the field takes the value outside this interval, the existing vortex configuration reconstructs, and a new configuration with different vorticity  $m'$  establishes (see Fig. 3). The jump on the magnetization curve may accompany such reconstruction. The new configuration may reveal either PME, or DME, depending on the resulting state characteristics. If the system may occupy only the ground state of minimal free energy, then no PME is possible, and the behavior  $M(H)$  should be completely reversible. The presence of PME and of the hysteresis is a signal of metastability. The examples of transitions between various metastable states are presented in Fig. 3, both for type-I and type-II superconductors.

The proposed qualitative GL-scenario looks rather general and one may attempt to apply it also to the case of HTS ( $\kappa \gg 1$ ), where PME is also observed in a field-cooling regime, is also characterized by the hysteresis, by the jump transitions between PME and DME branches of magnetization, and by the transitions between various quantum flux states (see, for instance, [14]). Whether PME in HTS can be explained by the presence of vortices, or by more exotic mechanisms, mentioned in the Introduction, is a question for further experimental and theoretical study.

#### V. ACKNOWLEDGMENTS

I am grateful to V.L. Ginzburg for the interest in this work. I also thank H.J. Fink, who pointed out to the paper [16], where the edge-suppressed states (discussed recently in [5]) were first encountered (see the footnote in [16]).

- 
- [1] A.K. Geim et al., Nature (London) **396**, 144 (1998); *ibid*, **390**, 259 (1997).
  - [2] V.V. Moshchalkov, X.G. Qiu, V. Bruyndoncx, Phys. Rev. **B55**, 11 793 (1997).
  - [3] J.J. Palacios, Phys. Rev. **B 58**, R5948 (1998); Phys. Rev. Lett. **84**, 1796 (2000).
  - [4] P. Singha Deo, F.M. Peeters, V.A. Schweigert, Supralatt.

- and Microstruct. **25**, 1195 (1999); Phys. Rev. B **59**, 6039 (1999).
- [5] G.F. Zharkov, V.G. Zharkov, A.Yu. Zvetkov (submitted to Phys. Rev.B).
- [6] F.B. Müller-Alinger, A.C. Motta, Phys. Rev. Lett. **84**, 3161 (2000).
- [7] L. Pust, L.E. Wenger, M. R. Koblishka, Phys. Rev.B **58**, 14 191 (1998).
- [8] G.F. Zharkov, V.G. Zharkov, Physica Scripta **57**, 664 (1998); G.F. Zharkov, V.G. Zharkov, A.Yu. Zvetkov, Phys. Rev. B **61**, 12 293 (2000).
- [9] D. Saint-James, P. de Gennes, Phys. Lett. **7**, 306 (1963).
- [10] D. Saint-James, Phys. Lett. **15**, 13 (1965).
- [11] V.L. Ginzburg, Zh. Exp. Teor. Fyz. **34**, 113 (1958); Soviet Phys.– JETP **7**, 78 (1958).
- [12] H.J. Fink, D.S. McLachlan and B. Rothberg-Bibby, in *Prog. in Low Temp. Phys.*, v. VIIb, p. 435–516, ed. D. F. Brewer, North Holland Pub., Amsterdam- New York- Oxford (1978).
- [13] A. Bezryadin, B. Pannettier, J. of Low Temp. Phys. **102**, 73, (1996).
- [14] W. Braunish et al., Phys. Rev. Lett. **68**, 1908 (1992).
- [15] A.E. Koshelev, A.I. Larkin, Phys. Rev.B **52**, 13 559 (1995).
- [16] H.J. Fink, A.G. Presson, Phys. Rev. **168**, 168 (1968).

### Figures captions

Fig. 1. The superconducting phase boundaries of vortex states with different vorticities  $m$  (the numerals at the curves). (a) –  $\varkappa = 2$ ; (b) –  $\varkappa = 1$ ; (c) –  $\varkappa = 0.5$ . The vertical dotted line  $h_\xi = 1$  corresponds to the critical field  $H_{c2}$ , the line  $h_\xi = 1.695$  corresponds to the critical field  $H_{c3}$ . (Here  $R_\lambda = R/\lambda$ ,  $h_\xi = H/H_\xi$ ,  $H_\xi = \phi_0/(2\pi\xi^2)$ .)

Fig. 2. (a) – The maximal value of the order parameter,  $\psi_{max}$ , in  $m$ -state; (b) – the magnetization ( $-4\pi M_\lambda$ ), Eq. (6);  $M_\lambda = M/H_\lambda$ ,  $H_\lambda = \phi_0/(2\pi\lambda^2)$ ; (c) – the normalized free-energy, Eq. (7), as functions of  $h_\xi$  for  $R_\lambda = 2$ ,  $\varkappa = 2$ .

Fig. 3. The same, as in Fig. 2, but for: (a, b, c) –  $R_\lambda = 2.5$ ,  $\varkappa = 1$ ; (d, e, f) –  $R_\lambda = 4$ ,  $\varkappa = 0.5$ . The letters  $\alpha, \beta, \gamma, \delta, \varepsilon$  mark the points, where  $m$ -solution terminates; the transitions to the nearest laying energy states are shown by the vertical arrows. The paramagnetic parts of the curves lay to the left of vertical lines, where  $M_\lambda = 0$ . [The arrows in Fig. 3(a) show the transition to the normal state ( $\psi = 0$ ). The arrows in Figs. 3(d) mark the possible hysteresis loop boundaries for the state  $m = 0$ :  $\gamma$  – superheated (*sh*) Meissner state,  $\delta$  – supercooled (*sc*) normal state.]

Fig. 4. The co-ordinate dependences: (a, d, g) – the order parameter  $\psi$ , (b, e, h) – the magnetic field  $b$ , (c, f, i) – the current  $j$ ; for solutions with different  $R_\lambda, \varkappa, m$  (see numbers in the insets). The curves 1 correspond to maximal paramagnetism ( $M > 0$ ), the curves 2 correspond to  $M = 0$ , the curves 3 correspond to maximal diamagnetism ( $M < 0$ ). The curves 1,2,3 are calculated for the following values of the applied field  $h_\lambda = H/H_\lambda$  ( $h_\lambda =$

$\varkappa^2 h_\xi$ ): 1 –  $h_\lambda = 1.52$ , 2 –  $h_\lambda = 2.921$ , 3 –  $h_\lambda = 4.30$  (if  $R_\lambda = 2$ ,  $\varkappa = 2$ ,  $m = 4$ ); 1 –  $h_\lambda = 0.45$ , 2 –  $h_\lambda = 0.985$ , 3 –  $h_\lambda = 1.52$  (if  $R_\lambda = 2.5$ ,  $\varkappa = 1$ ,  $m = 2$ ); 1 –  $h_\lambda = 0$ , 2 –  $h_\lambda = 0.195$ , 3 –  $h_\lambda = 0.48$  (if  $R_\lambda = 4$ ,  $\varkappa = 0.5$ ,  $m = 1$ ).

Fig. 5. Shown are as functions of temperature  $t = T/T_c$ : (a) – the maximal value of the order parameter,  $\psi_{max}$ ; (b) – the magnetization ( $-4\pi M_\lambda$ ); (c) – the normalized free-energy difference,  $\Delta g$ . [For  $m = 0, 1, 2, 3, 4$  and  $A = 3$  ( $\varkappa = 1$ ,  $R = 5.4 \cdot 10^{-5}$  cm,  $H = 100$  Oe), see Fig. 1(b) and Eq. (9).]

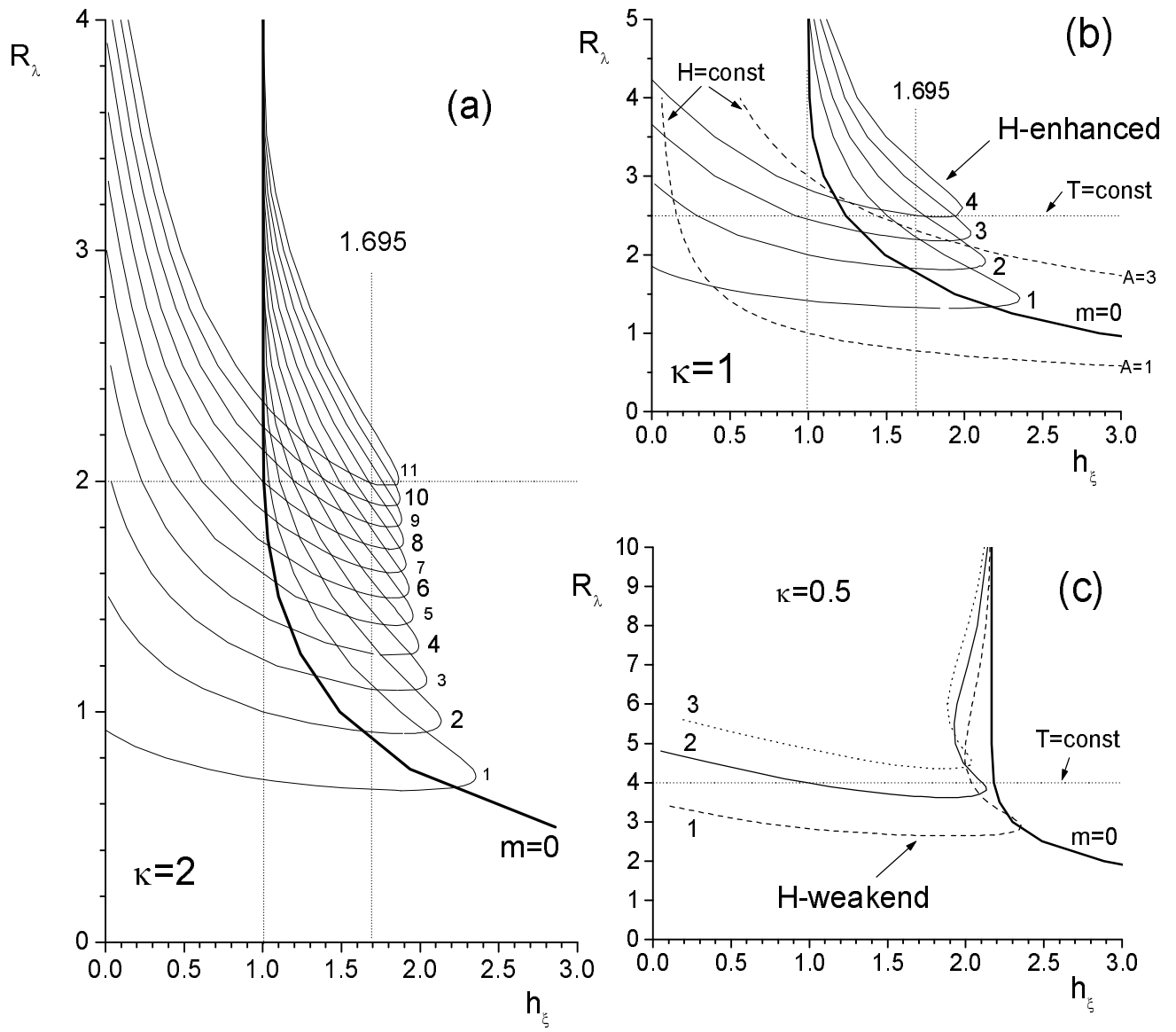


Fig. 1

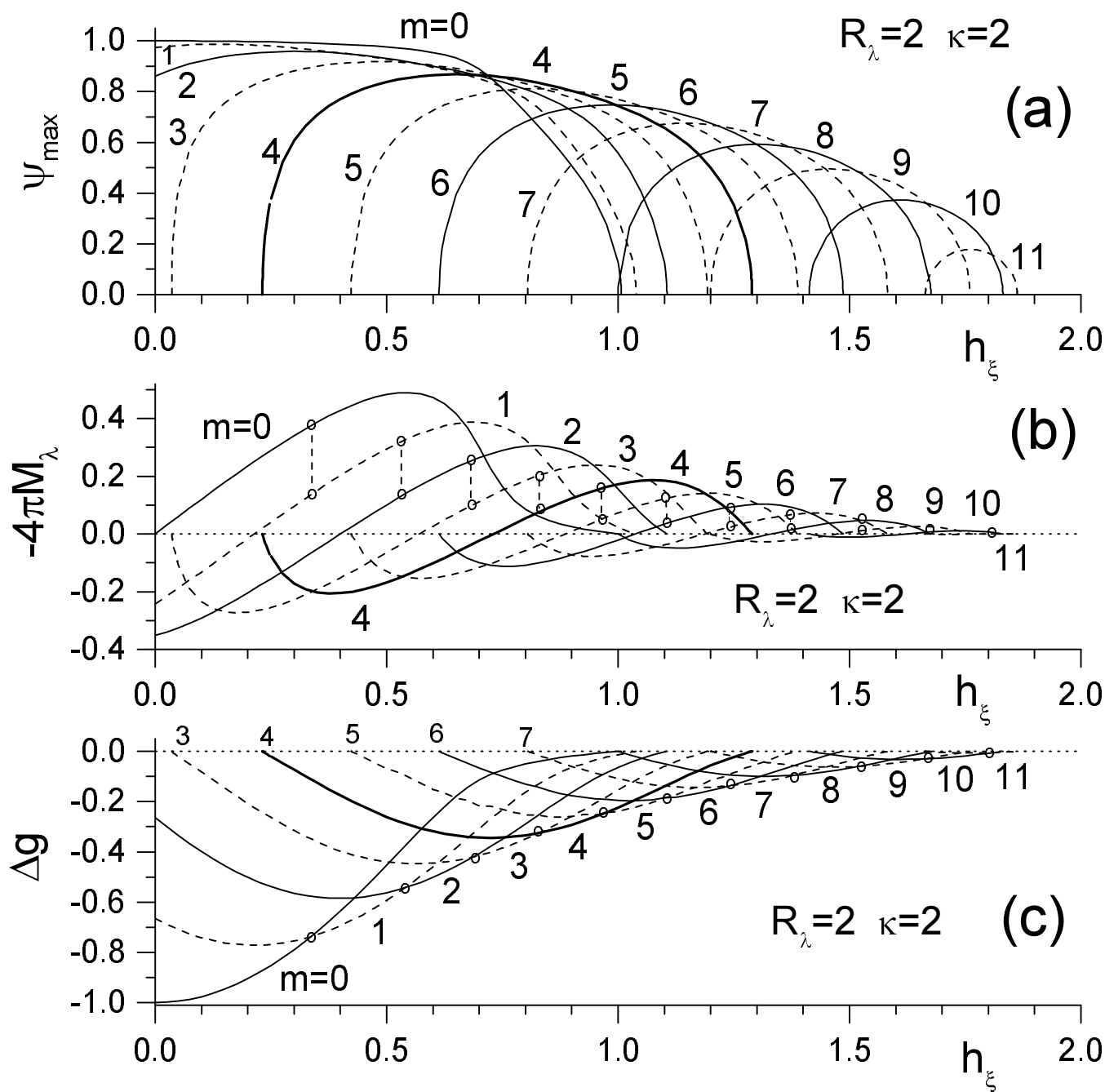


Fig. 2



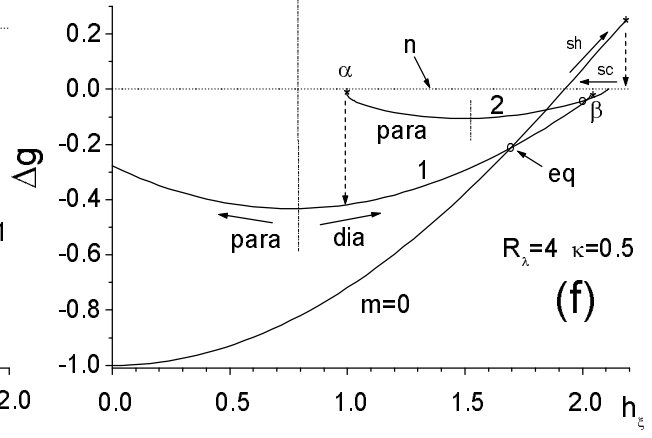
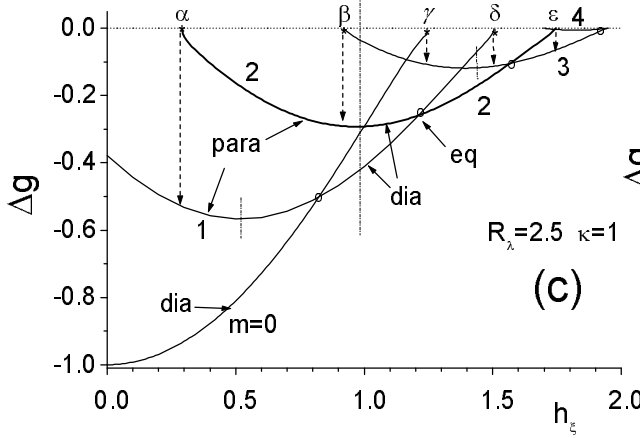
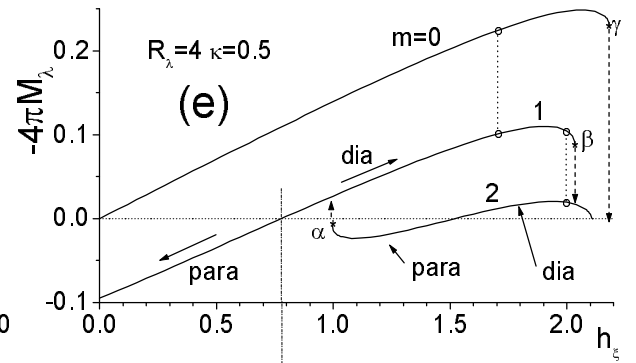
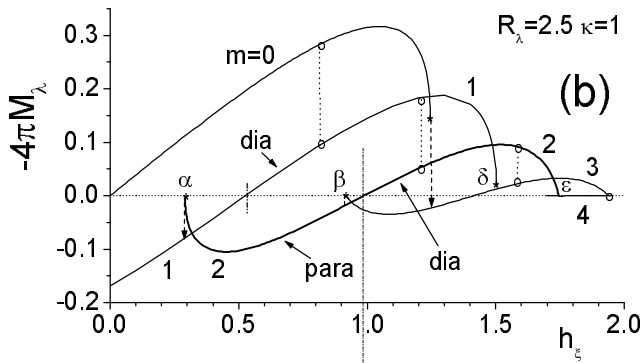
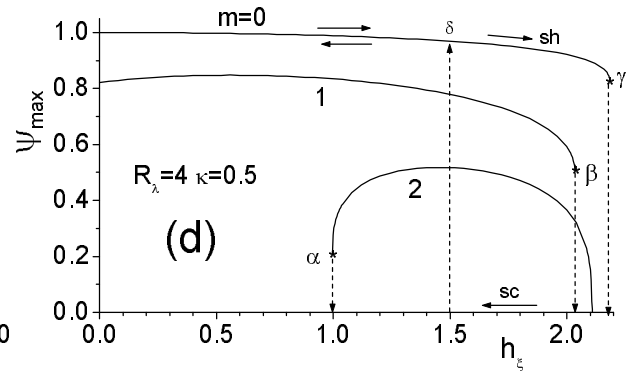
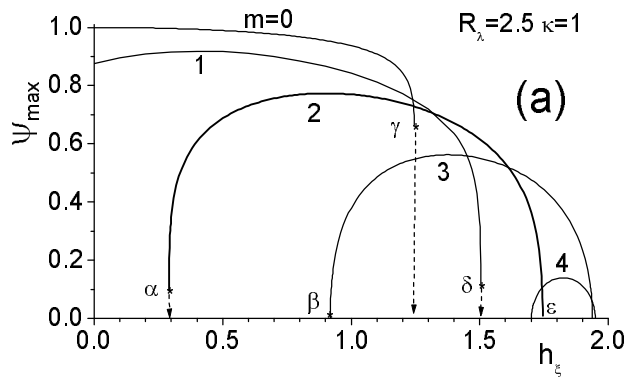


Fig. 3

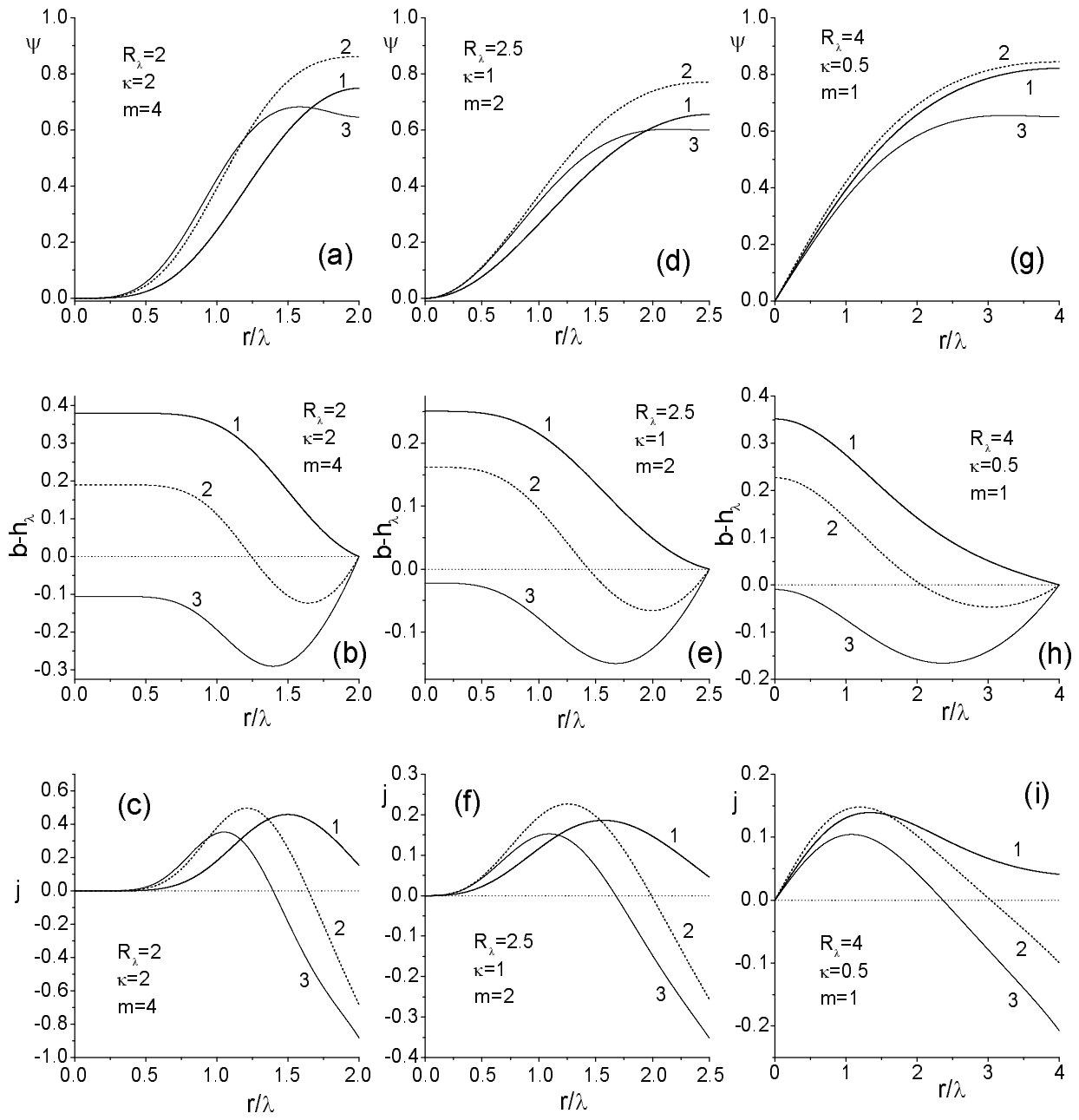


Fig. 4

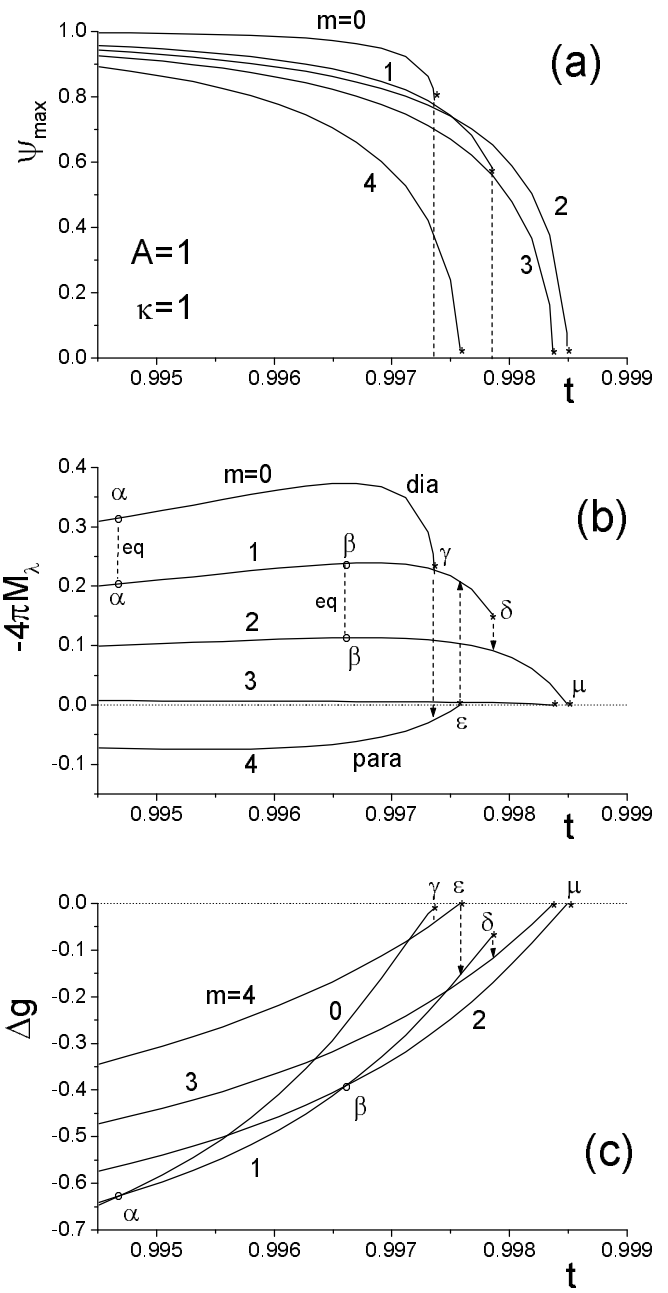


Fig. 5